Solar Energy Materials and Solar Cells 188 (2018) 177–181

Contents lists available at ScienceDirect

Solar Energy Materials and Solar Cells

journal homepage: www.elsevier.com/locate/solmat

6.6% efficient antimony selenide solar cells using grain structure control and an organic contact layer

Oliver S. Hutter*,[1], Laurie J. Phillips[1], Ken Durose, Jonathan D. Major

Stephenson Institute for Renewable Energy, Department of Physics, University of Liverpool, L69 7ZF Liverpool, UK

ARTICLE INFO

Keywords:
Antimony selenide
Sb_2Se_3
Photovoltaics
Solar cells
Thin film
Organic

ABSTRACT

We report a high efficiency antimony selenide (Sb_2Se_3) photovoltaic device structure using a new multi-step close space sublimation deposition process incorporating a Sb_2Se_3 seed layer; key to achieving higher efficiency devices via close space sublimation. Utilizing a glass|FTO|TiO_2|Sb_2Se_3|PCDTBT|Au structure, a peak efficiency of 6.6% was achieved, which is comparable to the current record devices for this material. Crucially, this device avoids toxic lead in the hole transport material, and cadmium in the window layer. Moreover, the addition of the PCDTBT back contact both maintains peak efficiency of 6.6%, and improves the uniformity of performance, increasing the average efficiency from 4.3% to 6.1%.

1. Introduction

Antimony selenide (Sb_2Se_3) is emerging as one of the most exciting new photovoltaic (PV) absorber materials, combining abundant, low toxicity constituents with rapidly improving efficiencies [1,2]. A near-direct bandgap of ~1.2 eV and a high absorption coefficient over much of the visible spectrum [2] means that it has the potential to outperform absorbers such as CdTe [3,4]. Its crystal structure comprises 1D $(Sb_4Se_6)_n$ ribbons [5,6] and thus the grains are terminated by van der Waals interactions rather than dangling covalent bonds, offering grain boundaries which are potentially benign [1,7,8]. This is evidenced by a large directional variability in hole mobilities [9]. Ribbons oriented perpendicular to the substrate should therefore offer improved charge transport and reduced recombination [9].

The first reported power conversion efficiency (PCE) of a functional Sb_2Se_3 PV device was 3.2% by Choi *et al.* in 2014, doubling to 6.5% for a CdS|Sb_2Se_3|PbS quantum dot device, the current record, by 2017 [10,11]. However, whilst further device efficiency improvements are of course required, it is also of importance to produce non-toxic device structures, in order not to undermine the use of a non-toxic absorber layer. As an example, CdS is a highly toxic source of cadmium [12], and thus should be avoided if possible. Sb_2Se_3 is commonly reported to have a low carrier concentration [1,13], hence recent literature reports using a PIN device structure, partnering the quasi-intrinsic absorber with n-type electron and p-type hole extraction layers to enhance charge extraction [10]. Recent work by our group was the first to demonstrate the efficacy of close space sublimation (CSS) as a deposition route for Sb_2Se_3 for photovoltaics [3]. CSS is highly promising for Sb_2Se_3 as it yields large grains with preferred orientation, and importantly the ability to control the grain structure.

In this work we report on improved Sb_2Se_3 cell performance to world leading levels via a two-stage CSS deposition to generate a compact "seed" layer prior to the deposition of large Sb_2Se_3 grains. Furthermore, a significant improvement in uniformity was achieved by including a hole transport material (HTM). A TiO_2 layer was employed as the electron extraction layer while poly[N-9′-heptadecanyl-2,7-carbazole-*alt*-5,5-(4′,7′-di-2-thienyl-2′,1′,3′- benzothiadiazole)] (PCDTBT) was selected as the optional HTM due to the position of its ionization potential and electron affinity at 5.4 and 3.6 eV respectively [14]. Photo-oxidation is known to generate sub-bandgap states close in energy to the valence band of Sb_2Se_3 and therefore allow efficient hole extraction [15,16]. The LUMO is also high enough to block the transfer of minority carriers (electrons) from the Sb_2Se_3 to Au and thereby reduce recombination at the back-contact (Fig. S1) [14].

2. Materials and methods

FTO-coated glass substrates (TEC10, NSG Ltd.) were spin coated with 0.15 M and 0.3 M titanium isopropoxide in ethanol at 3000 rpm for 30 s, and dried after each deposition at 120°C under N_2. The substrates were then annealed in air at 550°C for 30 min and cooled rapidly to create compact titania layers [17]. The Sb_2Se_3 layers were grown via

* Corresponding author.
E-mail address: ohutter@liverpool.ac.uk (O.S. Hutter).
[1] These authors contributed equally to this work.

https://doi.org/10.1016/j.solmat.2018.09.004
Received 16 May 2018; Received in revised form 30 August 2018; Accepted 3 September 2018
Available online 10 September 2018

CSS in a novel two step process. First a compact seed layer was grown for 5 mins at 0.05 mbar, with a source temperature of 350°C, followed by annealing for 10 mins in 260 mbar N_2. Secondly, a 30 min growth step was carried out at a source temperature of 450°C and pressure of 13 mbar to produce a more compact and orientated grain structure, similar to previous work on CdTe [18]. The substrate was then cooled rapidly with N_2. Where included, PCDTBT was spin-cast in air at 6000 rpm for 60 s from a 4 mg/mL solution in chloroform. Cells were completed by thermally evaporating 100 nm of gold through a shadow mask to define 0.1 cm^2 contacts and JV measurements were recorded under AM1.5 conditions using a TS Space Systems AAA100 solar simulator calibrated with a photodiode. 48 devices of each type were fabricated. SEM images were taken using a JEOL 7001 FEGSEM, X-Ray Diffraction (XRD) was carried out using a Rigaku Smartlab and AFM measurements were carried out using a Veeco diInnova AFM in tapping mode. UV/Vis spectra were recorded using a Shimadzu Solid Spec 3700 UV–Vis spectrophotometer and an integrating sphere.

3. Results and discussion

3.1. Sb_2Se_3 seed layer

Fig. 1a shows a top-down SEM image of the initial low-temperature seed layer. The seed layer is compact, yielding a high density of nucleation points for the second stage of growth, similar to work on CdTe [19]. The seed layer also serves to prevent shorting pathways between large CSS grains of the final film and increase the shunt resistance. Optical transmission measurements show a bandgap of ~1.3 eV and very high absorption (Fig. 1b) for this seed layer. The thickness of this seed layer was found to be 66 ± 8 nm using cross sectional AFM (Fig. 1c). The XRD pattern (Fig. 1d) shows preferred crystal structure orientation, confirmed by the lack of a significant (120) peak around 17°, but a strong (211) peak at 28.4°. This indicates that the 1D ribbons are mostly tilted on the substrate, which although not ideal for carrier transport is preferred to ribbons parallel to the substrate (120) [1,7,10]. The largest peak in the XRD pattern comes from the FTO glass [20], as both the titania and seed layers are very thin compared to the X-ray penetration depth. Single stage CSS-deposited Sb_2Se_3 films typically have pinholes leading to a lower fill factor [3]. The combination of these properties mean that the seed layer is thus a key feature for achieving higher efficiency Sb_2Se_3 devices via CSS, and has improved the device performance by over 1% absolute compared to similar control devices without this seed layer, as explained in Section 3.3. The seed layer in isolation as a sole absorber material did not produce a working device due to a very thin absorber thickness creating a high number of shunting pathways.

3.2. Complete Sb_2Se_3 layer

Fig. 2a shows an SEM image of the complete Sb_2Se_3 layer after both stages of CSS growth. This two-stage approach generates large columnar Sb_2Se_3 grains of ≈ 2 μm diameter. These grains are packed tighter, more uniformly orientated and thereby minimize pinholes within the Sb_2Se_3 film compared to a film without the seed layer (Fig. S2). The device cross-sectional SEM image (Fig. 2c) shows that the Sb_2Se_3 grain height (≈1.5 μm) is sufficient to span the full thickness of the device and connect the TiO_2 and the PCDTBT layers without lateral grain boundaries that could impede charge transport. EDX analysis confirmed the composition as being stoichiometric Sb_2Se_3 within experimental error (Fig. S3) while optical transmission measurements show a bandgap of ~1.2 eV and high absorption (Fig. 2b), similar to previously reported values [1,2,8,21]. A difference in band gap and absorption coefficient is observed between the seed and final layers, indicating that the seed layer is likely consumed during the second growth stage. As the seed layer has a continuous slab like morphology which is very morphologically distinct to the full Sb_2Se_3 film, a large difference in absorption coefficient would be expected. Anisotropic optical absorption properties with ribbon orientation are also predicted for Sb_2Se_3 [22,23]. The Sb_2Se_3 film XRD pattern (Fig. 2c) shows a preferred crystal structure orientation, confirmed by the lack of a significant (120) peak around 17°, but strong (211) and (221) peaks at 28.4° and 31.4° respectively. This indicates the 1D ribbons are mostly predominantly inclined with respect to the substrate, which is beneficial for carrier transport [1,7,10]. It also indicates that the Sb_2Se_3 seed layer may be acting a templating layer for vertical ribbon growth, although the (211) peak is more intense in the final film compared to the

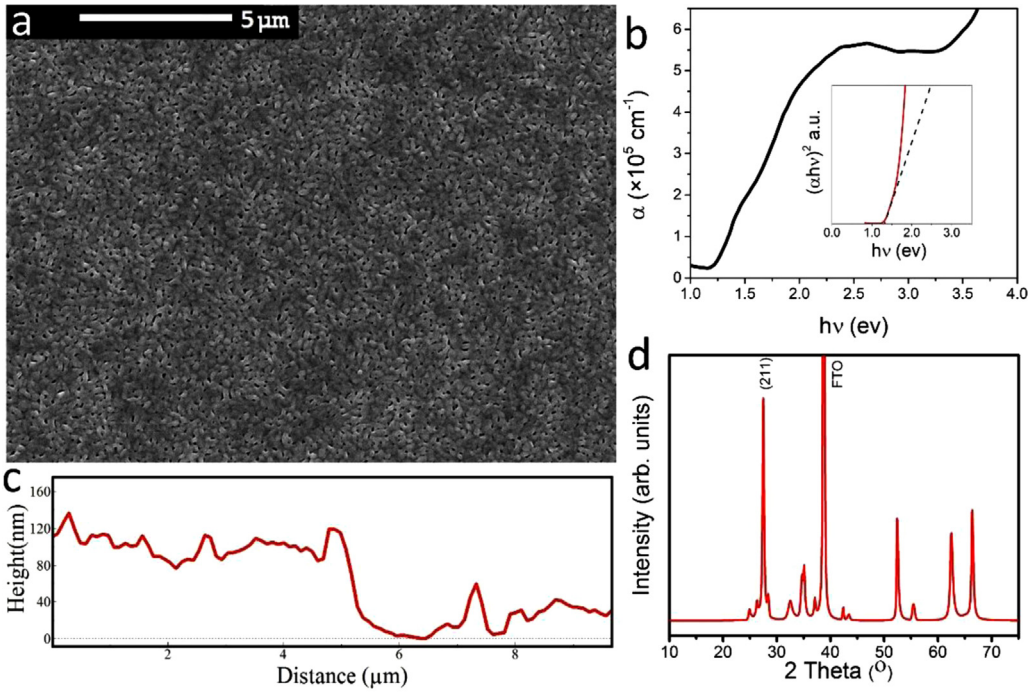

Fig. 1. Sb_2Se_3 seed layer characteristics: (a) Top-down SEM image, (b) Absorption coefficient and Tauc plot (inset), (c) AFM cross section, (d) XRD pattern.

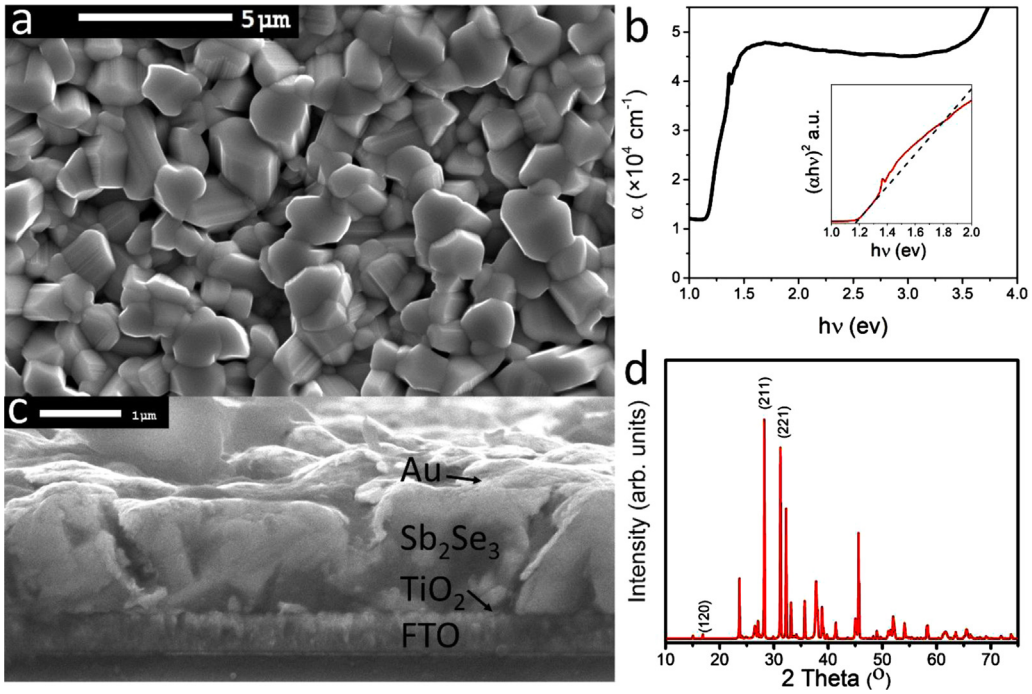

Fig. 2. Complete Sb_2Se_3 film characteristics: (a) Top down SEM image, (b) Absorption coefficient and Tauc plot (inset), (c) Device cross section SEM image, (d) XRD pattern.

seed layer. Bilayer thin film structures for other photovoltaic materials have been investigated previously and are established for materials such as CdTe [24,25], although not for Sb_2Se_3.

3.3. PV devices

In this work, the base device structure used for cell fabrication was: glass|FTO|TiO_2|Sb_2Se_3|Au. The peak JV performance of devices with and without a Sb_2Se_3 seed layer are shown in Fig. 3a, with average and peak values in Table S1. The peak device without a Sb_2Se_3 seed layer achieved a V_{oc}, J_{sc}, *FF* and *PCE* of 0.401 V, 28.34mAcm^{-2}, 43.8% and 4.96% respectively. The seed layer improves the peak device performance by over 1% absolute, from 4.96% without a seed layer, to 6.56% with a seed layer. The majority of this improvement arises through increased current density. Fig. 3b compares devices with a seed layer (denoted "*Au*"), to devices including PCDTBT and a seed layer: glass|FTO|TiO_2|Sb_2Se_3|PCDTBT|Au (denoted "*P-Au*").Table 1 shows the average and peak parameters for these devices, whilst Fig. 3b shows the peak JV performance.

The seed layer produces a denser, more compact, film morphology in the Sb_2Se_3 films which leads to a large increase in PCE of over 1%. The addition of a PCDTBT contact layer only marginally increases the peak performance to 6.6%, but it drastically improves the average device characteristics (Table 1). The number of devices that failed due to a short circuit is also greatly reduced with PCDTBT. Individual pinhole free pixels are still possible without PCDTBT, and this explains why the peak "*Au*" PCE is similar to the "*P-Au*" cells. In previous work, Poly ({4,8-bis[(2-ethylhexyl)oxy] benzo[1,2-b:4,5-b′]dithiophene-2,6-diyl} {3-fluoro-2-[(2-ethylhexyl)carbonyl] thieno[3,4-b]thiophenediyl}) (PTB7) has also been used as a contacting layer for Sb_2Se_3 cells, but yielded poor performance in comparison to PCDTBT [26]. P3HT can also be used as a contacting layer for Sb_2Se_3 cells [3]. The improved average device characteristics in this work can be explained by PCDTBT acting as an effective pinhole-blocking layer [27], which increased V_{oc} and *FF*, whilst the small decrease in J_{sc} may be due to the polymer introducing a slight resistive barrier. Various spin speeds for PCDTBT were used, from 500 to 6000 rpm, with the average PCE values increasing from 1.67 ± 0.9% for 500 rpm, to 6.1 ± 0.5% for 6000 rpm. 6000 rpm was then used for all subsequent runs. This shows that at lower spin speeds, the PCDTBT layer was too thick and introduced a resistive barrier into the device. Various PCDTBT concentrations were also investigated, with the average PCE of devices for 2, 4, and 5 mg/mL of PCDTBT in chloroform being 4.26%, 6.06% and 3.55% respectively when spin coated at 6000 rpm. This demonstrates that PCDTBT coverage is a balance between covering the pin holes which affect the performance negatively in the device, and making the PCDTBT layer too resistive within the device. The external quantum efficiency (EQE) of both "*P-Au*" and "*Au*" (Fig. 3c), peaks at 80%, with a rapid rise and square shape at low wavelengths indicating low parasitic absorption from TiO_2. However, the long slope below the bandgap at ~1030 nm indicates significant band tailing and the presence of defects [9]. The devices show very similar EQE shapes, with no contribution from PCDTBT to photocurrent at around 400 and 570 nm [28]. This demonstrates that the Sb_2Se_3 layers used in this work are highly absorbing and very little light gets past the Sb_2Se_3 through to the PCDTBT layer; the PCDTBT layer is acting only as a pinhole blocking layer, and not as an absorber layer within the device. The carrier concentration, measured using capacitance-voltage (C-V) profiling, (Fig. 3d) shows a carrier concentration in excess of 10^{16} cm^{-3}. This is higher than many literature reports [1,29,30,31] and explains why the "*Au*" sample using this material is able to perform as well as the "*P-Au*" device. The peak performances of both "*P-Au*" and "*Au*" devices with efficiencies of 6.56% and 6.54% respectively are equivalent to the highest efficiency values reported for Sb_2Se_3 without including the toxic lead from the PbS quantum dot HTM, and the cadmium from the CdS window layer in the previous record devices [11].

4. Conclusions

In this study, we have demonstrated a novel two-stage CSS deposition method as a viable technique for producing high quality films suitable for PV devices, and that a seed layer is a crucial step in producing CSS deposited Sb_2Se_3 films of high quality. 6.6% efficient Sb_2Se_3 devices with commensurate efficiency to current record devices are

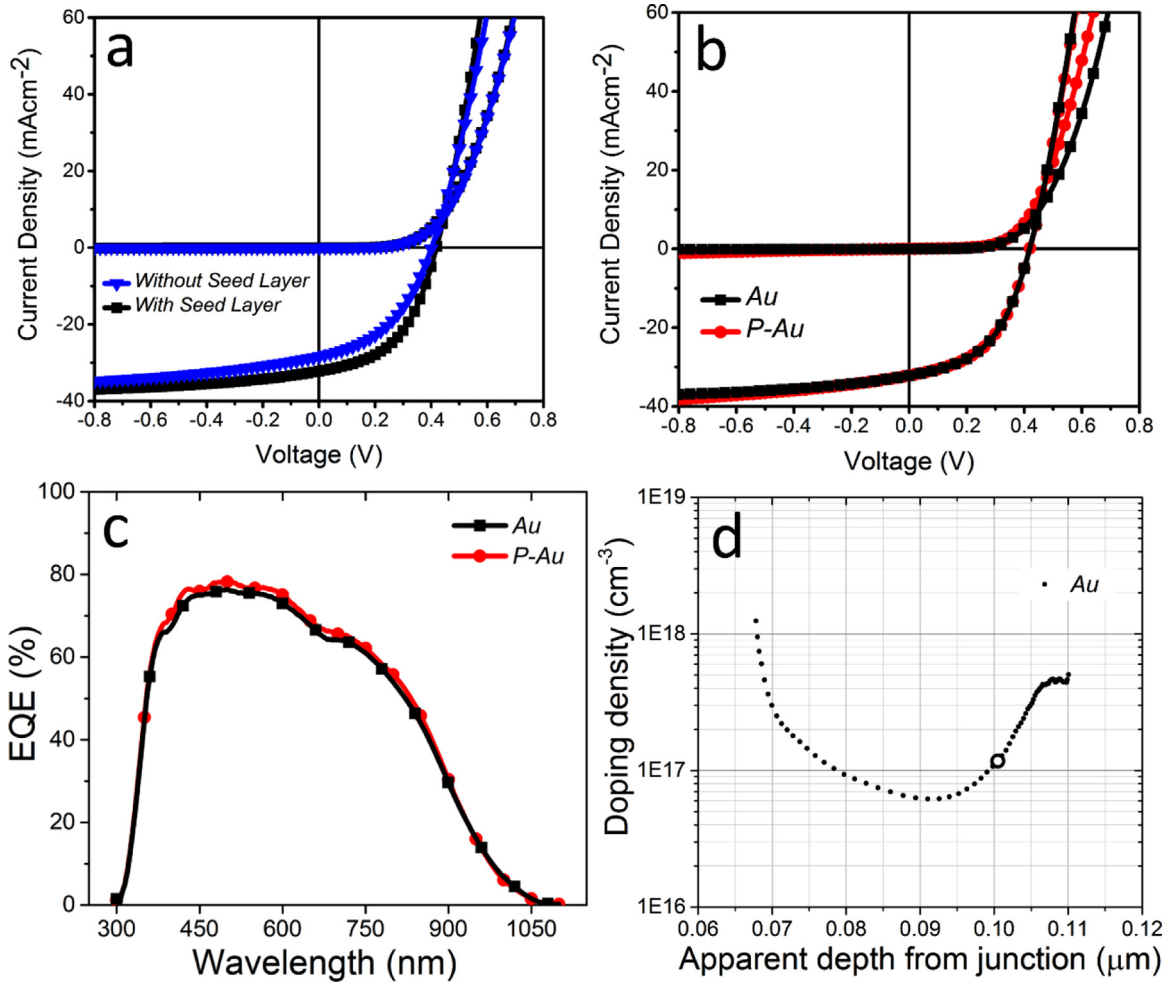

Fig. 3. (a) JV scans of Sb_2Se_3 devices with and without a seed layer, (b) JV scans of "*Au*" and "*P-Au*" Sb_2Se_3 devices (both with a seed layer), (c) EQE of "*Au*" and "*P-Au*" devices, (d) Depth-density profile from CV measurements of the "*Au*" device (circle denotes 0 V).

Table 1
Peak and average performance for Sb_2Se_3 devices with a PCDTBT contact layer ("*P-Au*") and without ("*Au*"). Both types of devices utilize a Sb_2Se_3 seed layer.

Cell	V_{oc} / V	J_{sc} / mAcm^{-2}	*FF* / %	PCE / %
Peak "*Au*"	0.418	32.2	48.4	6.54
Average "*Au*"	0.36 ± 0.03	31.5 ± 0.9	37.3 ± 6.0	4.3 ± 1.2
Peak "*P-Au*"	0.419	32.2	48.5	6.56
Average "*P-Au*"	0.42 ± 0.01	29.9 ± 1.4	48.6 ± 2.2	6.1 ± 0.5

shown, without requiring the toxic lead from the lead sulfide quantum dots and the toxic Cd from the CdS window layer [11]. Additionally, by redesigning the cell structure to incorporate a PCDTBT layer, uniformity of performance is vastly improved without any loss in peak performance.

Acknowledgements

This work was supported by EPSRC grants EP/N014057/1 and EP/M024768/1. We thank S. Mariotti for helpful discussions.

Conflict of interests

The authors declare no competing financial interest.

Appendix A. Supplementary material

Supplementary data associated with this article can be found in the online version at doi:10.1016/j.solmat.2018.09.004.

References

[1] K. Zeng, D.-J. Xue, J. Tang, Antimony selenide thin-film solar cells, Semicond. Sci. Technol. 31 (2016) 63001.
[2] C. Chen, W. Li, Y. Zhou, C. Chen, M. Luo, X. Liu, K. Zeng, B. Yang, C. Zhang, J. Han, J. Tang, Optical properties of amorphous and polycrystalline Sb_2Se_3 thin films prepared by thermal evaporation, Appl. Phys. Lett. (2015) 43905.
[3] L.J. Phillips, C.N. Savory, O.S. Hutter, P.J. Yates, H. Shiel, S. Mariotti, L. Bowen, M. Brikett, K. Durose, D.O. Scanlon, J.D. Major, Current enhancement through a TiO_2 window layer for CSS-deposited Sb_2Se_3 solar cells, Submitt. IEEE J. Photovolt. (2018).
[4] S. Rühle, Tabulated values of the Shockley-Queisser limit for single junction solar cells, Sol. Energy 130 (2016) 139.
[5] M.R. Filip, C.E. Patrick, F. Giustino, GW quasiparticle band structures of stibnite, antimonselite, bismuthinite, and guanajuatite, Phys. Rev. B - Condens. Matter Mater. Phys. 87 (2013) 1.
[6] Y. Zhou, M. Leng, Z. Xia, J. Zhong, H. Song, X. Liu, B. Yang, J. Zhang, J. Chen, K. Zhou, J. Han, Y. Cheng, J. Tang, Solution-processed antimony selenide heterojunction solar cells, Adv. Energy Mater. 4 (2014) 4.
[7] Y. Zhou, L. Wang, S. Chen, S. Qin, X. Liu, J. Chen, D.-J. Xue, M. Luo, Y. Cao, Y. Cheng, E.H. Sargent, J. Tang, Thin-film Sb_2Se_3 photovoltaics with oriented one-dimensional ribbons and benign grain boundaries, Nat. Photonics 9 (2015) 409.
[8] W. Yang, J. Ahn, Y. Oh, J. Tan, H. Lee, J. Park, H.-C. Kwon, J. Kim, W. Jo, J. Kim, J. Moon, Adjusting the anisotropy of 1D Sb_2Se_3 nanostructures for highly efficient photoelectrochemical water splitting, Adv. Energy Mater. (2018) 1702888.
[9] C. Chen, D.C. Bobela, Y. Yang, S. Lu, K. Zeng, C. Ge, B. Yang, L. Gao, Y. Zhao, M.C. Beard, J. Tang, Characterization of basic physical properties of Sb_2Se_3 and its relevance for photovoltaics, Front. Optoelectron. 10 (2017) 18.

[10] Y.C. Choi, T.N. Mandal, W.S. Yang, Y.H. Lee, S.H. Im, Sb_2Se_3 -sensitized inorganic–organic heterojunction solar cells fabricated using a single-source precursor, Angew. Chem. (2014) 1329.
[11] C. Chen, L. Wang, L. Gao, D. Nam, D. Li, K. Li, Y. Zhao, C. Ge, H. Cheong, H. Liu, H. Song, J. Tang, 6.5% Certified efficiency Sb_2Se_3 solar cells using pbs colloidal quantum dot film as hole-transporting layer, ACS Energy Lett. 2 (2017) 2125.
[12] J.D. Major, R.E. Treharne, L.J. Phillips, K. Durose, A. Low-cost Non-toxic, Post-growth activation step for CdTe solar cells, Nature 511 (2014) 334.
[13] M.A. Tumelero, R. Faccio, A.A. Pasa, Unraveling the native conduction of trichalcogenides and its ideal band alignment for new photovoltaic interfaces, J. Phys. Chem. C. 120 (2016) 1390–1399.
[14] S.K. Lee, J.M. Cho, Y. Goo, W.S. Shin, J.-C. Lee, W.-H. Lee, I.-N. Kang, H.-K. Shim, S.-J. Moon, Synthesis and characterization of a Thiazolo[5,4-d]thiazole-based copolymer for high performance polymer solar cells, Chem. Commun. 47 (2011) 1791.
[15] C.H. Peters, I.T. Sachs-Quintana, W.R. Mateker, T. Heumueller, J. Rivnay, R. Noriega, Z.M. Beiley, E.T. Hoke, A. Salleo, M.D. McGehee, High efficiency polymer solar cells with long operating lifetimes, Adv. Mater. 24 (2012) 663.
[16] A. Tournebize, P.O. Bussière, P. Wong-Wah-Chung, S. Thérias, A. Rivaton, J.L. Gardette, S. Beaupré, M. Leclerc, Impact of UV–visible light on the morphological and photochemical behavior of a low-bandgap Poly(2,7-Carbazole) derivative for use in high-performance solar cells, Adv. Energy Mater. 3 (2013) 478.
[17] S. Mariotti, O.S. Hutter, L.J. Phillips, P.J. Yates, B. Kundu, K. Durose, Stability and performance of $CsPbI_2Br$ thin films and solar cell devices, ACS Appl. Mater. Interfaces 10 (2018) 3750.
[18] J.D. Major, Y.Y. Proskuryakov, K. Durose, G. Zoppi, I. Forbes, Control of grain size in sublimation-grown CdTe, and the improvement in performance of devices with systematically increased grain size, Sol. Energy Mater. Sol. Cells 94 (2010) 1107.
[19] J.D. Major, K. Durose, Early stage growth mechanisms of CdTe thin films deposited by close space sublimation for solar cells, Sol. Energy Mater. Sol. Cells 95 (2011) 3165.
[20] S.-L. Chen, J. Tao, H.-J. Tao, Y.-Z. Shen, A.-C. Xu, F.-X. Cao, J.-J. Jiang, T. Wang, L. Pan, In situ synthesis of two-dimensional leaf-like Cu_2ZnSnS_4 plate arrays as a Pt-free counter electrode for efficient Dye-sensitized solar cells, Green. Chem. 18 (2016) 2793.
[21] L. Wang, M. Luo, S. Qin, X. Liu, J. Chen, B. Yang, M. Leng, D. Xue, Y. Zhou, L. Wang, M. Luo, S. Qin, X. Liu, J. Chen, B. Yang, Ambient CdCl2 treatment on CdS buffer layer for improved performance of Sb_2Se_3 Thin film photovoltaics, Appl. Phys. Lett. (2015) 143902.
[22] TheodoreD.C. Hobson, OliverS. Hutter, Max Birkett, TimD. Veal, Ken Durose, Growth and Characterization of Sb2Se3 Single Crystals for Fundamental Studies, WCPEC-7 Conference Paper, 2018.
[23] R. Vadapoo, S. Krishnan, H. Yilmaz, C. Marin, Electronic structure of antimony selenide (Sb2Se3) from GW calculations, Phys. Status Solidi Basic Res. 248 (2011) 700.
[24] V. Krishnakumar, A. Barati, H.J. Schimper, A. Klein, W. Jaegermann, A possible way to reduce absorber layer thickness in thin film CdTe solar cells, Thin Solid Films. 535 (2013).
[25] J. Han, C. Spanheimer, G. Haindl, G. Fu, V. Krishnakumar, J. Schaffner, C. Fan, K. Zhao, A. Klein, W. Jaegermann, Optimized chemical bath deposited CdS layers for the improvement of CdTe solar cells, Sol. Energy Mater. Sol. Cells 95 (2011) 816–820.
[26] O.S. Hutter, L.J. Phillips, P. Yates, J.D. Major, K. Durose, CSS antimony selenide film morphology and high efficiency PV devices, WCPEC-7 Conference Paper, 2018.
[27] J.D. Major, L.J. Phillips, M. Al Turkestani, L. Bowen, T.J. Whittles, V.R. Dhanak, K. Durose, P3HT as a pinhole blocking back contact for CdTe thin film solar cells, Sol. Energy Mater. Sol. Cells 172 (2017) 1.
[28] S.-W. Baek, J. Noh, C.-H. Lee, B. Kim, M.-K. Seo, J.-Y. Lee, Plasmonic forward scattering effect in organic solar cells: a powerful optical engineering method, Sci. Rep. 3 (2013) 1726.
[29] C. Chen, Y. Zhao, S. Lu, K. Li, Y. Li, B. Yang, W. Chen, L. Wang, D. Li, H. Deng, F. Yi, J. Tang, Accelerated optimization of TiO_2/Sb_2Se_3 thin film solar cells by high-throughput combinatorial approach, Adv. Energy Mater. (2017) 1700866.
[30] L. Wang, D.-B. Li, K. Li, C. Chen, H.-X. Deng, L. Gao, Y. Zhao, F. Jiang, L. Li, F. Huang, Y. He, H. Song, G. Niu, J. Tang, Stable 6%-efficient Sb_2Se_3 Solar Cells with a ZnO Buffer Layer, Nat. Energy 2 (2017) 17046.
[31] M. Luo, M. Leng, X. Liu, J. Chen, C. Chen, S. Qin, J. Tang, Thermal evaporation and characterization of superstrate $CdS/Sb2_Se3$ solar cells, Appl. Phys. Lett. (2015) 173904.